Answers to reviewer 1

We thank the reviewer for his/her constructive remarks. In the manuscript we identified all changes in response to the reviewer in **black bold**.

General comments

Figures 4, 7, and 16 were replotted and enlarged as suggested.

Figures 2, 3, and 5 were replotted to be similar to Fig. 12 as suggested.

Figs. 10 and 11 are vector plots and a polar-stereographic projection doesn't work well due to the convergence of meridians toward the pole. Fig. 10 was replotted.

We explained all abbreviations about the Target and Taylor diagramms in Fig. 6 by improved figure caption: **Figure 6. Target diagram (a) of normalised bias and normalized unbiased root-mean-square difference (uRMSD) and Taylor diagram (b) of normalised standard deviation and correlation between the RASM sea ice thickness simulations and CryoSat2/SMOS data from November 2019 to March 2020. The square marker indicates the reference (REF) value, i.e., perfect model.**

We introduced the following sentences for description of the Target and Taylor diagramms: **RASM skill is assessed using the Target diagram (Joliff et al., 2009) to visualise root-mean-square difference (RMSD; distance from a center), unbiased RMSD (uRMSD; x-axis), and bias (y-axis) for monthly SIT on a single plot. They are normalised by the standard deviation of CryoSat2/SMOS SIT. The Taylor diagram (Taylor, 2001) provides an additional set of statistics in uRMSD by displaying the correlation and the ratio of the standard deviation between RASM and CryoSat2 SIT**

We added the following citations:

Jolliff, J. K., J. C. Kindle, I. Shulman, B. Penta, M. A. M. Friedrichs, R. Helber, and R. A. Arnone (2009), Summary diagrams for coupled hydrodynamic-ecosystem model skill assessment, J. Mar. Syst., 76, 64–82.

Taylor, K. E. (2001), Summarizing multiple aspects of model performance in a single diagram, J. Geophys. Res., 106, 7183–7192.

Summary and conclusion sections were partly revised.

Specific comments:

LN 165-167: We described the concept in the text**. The concept is described by *Ricker (2020)* in the CryoSat2-SMOS merged product description document. An optimal interpolation scheme (OI) has been used, that allows the merging of datasets from diverse sources on a predefined analysis grid. The data are weighted differently based on known uncertainties of the individual products and an estimated correlation length scale. OI minimizes the total error of observations with respect to a background field and provides ideal weighting for the observations at each grid cell. The background field consists of a weighted average of CryoSat-2 and SMOS data two weeks before and after the rolling observation period with a length of 7 days. The CryoSat2-SMOS product is then defined as the sea-ice thickness analysis fields of the 7 day observation period**

with the center date as the reference time of each file. Melting does not allow to retrieve sea-ice thickness estimates from CryoSat-2 and SMOS during summer between May and September. Therefore, the merged product is limited to the period from mid-October to mid-April only due to the background field requirement.

LN 208: Title of section 3.1 was changed to: **3.1 Analysis of atmospheric and sea ice conditions in ERA5 and satellite data**

LN 216: In Fig. 1a we explain the AO time series and in Fig. 1b the spatial AO pattern.

We explain with the following text why Fig. 1b is based on ERA-5 1979-2000.

Figure 1a presents daily values of the AO index in mean sea level pressure (SLP) based on ERA-5 from October 2019 until May 2020 with 7-day running mean (red line) and Fig. 1b the spatial AO pattern north of 20 °N. The AO pattern was defined as the leading mode of Empirical Orthogonal Function analysis of monthly mean SLP during the 1979-2000 period over the domain 20°-90°N. This domain and reference period was used for the calculation of the spatial AO patterns to ensure a comparability with the widely used AO index provided by the NOAA Climate Prediction center (CPC, https://www.cpc.ncep.noaa.gov/products/precip/CWlink/daily_ao_index/ao.shtml), which is based on the AO pattern calculated for the mentioned reference period and NCEP/NCAR reanalysis data set. The daily AO indices (Fig. 1a) have been obtained by projecting ERA5 daily SLP data from 1979 to May 2020 onto the AO pattern shown in Fig. 1b. For comparison the loading pattern of the AO for the different ERA-5 reference period 2010-2019 was computed (not shown), and the corresponding AO index for the MOSAiC period, obtained by projecting the daily SLP anomalies onto this loading pattern. The time series of daily values of the AO index from October 2019 to April 2020 obtained by projecting the daily SLP anomalies onto the loading pattern from 2010-2019 agree entirely with Fig 1a.

For the information of the reviewer (not presented in the manuscript), we display in Fig. R1a the AO pattern for the period 2010-2019 and in Fig. R1b the AO time series of by projecting onto the loading pattern shown in Fig. R1a.

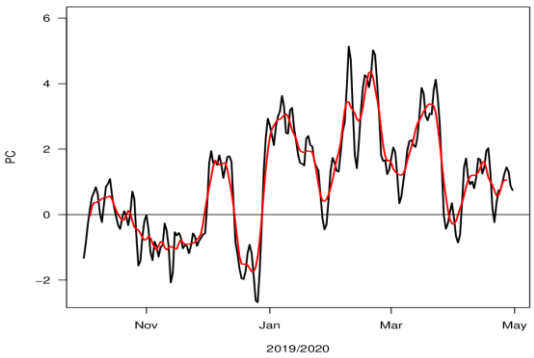

Fig. R1a.Time series of daily values of the AO index from October 2019 to April 2020 (black line) with 7-day running mean (red line), obtained by projecting the daily SLP anomalies onto the loading pattern shown in Fig. R1b.

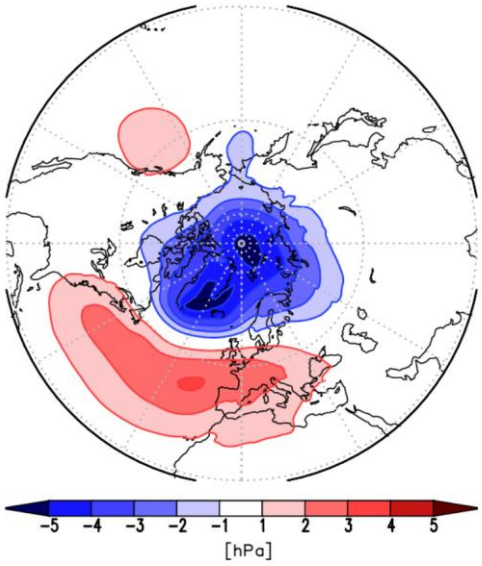

Figure R1b. Loading pattern of AO based on monthly mean SLP for the period 2010-2019 (ER5 data).

LN 219: Fig. 2 was revised

LN 255-257: Figs. 3 and 4 have been replotted using the same color bars. The mentioned sentence was changed to: **The largest positive thickness anomalies between 1.0 and 1.5 m occur in the BS, along the north-eastern Canadian coast and in the central Arctic Ocean.**

LN 265-267: The sentence was changed to: **Sea ice thickness has been measured by satellite radar altimeters. The synthetic aperture radar capability enables CryoSat-2 to measure sea ice freeboard at a great resolution and precision. Sea ice freeboard is the portion of the floating ice above sea level and is estimated from the elevation difference between radar echoes backscattered from sea ice and ocean tie-points between sea-ice floes. The freeboard measurements are converted to sea ice thickness with knowledge of the densities of sea ice, ocean water, and snow, and estimating the depth of snow accumulated on the ice surface based on climatological values (Hendricks et al. 2020).**

LN 274: **The domain averaged bias is the difference between RASM and satellite data in the region shown in Fig. 12, including all the ice regions with boundaries at DS (Davis Street), FS (Fram Strait), BSO (Barents Sea Opening) and BS (Bering Strait).**

LN 277: The sentence was changed to: **The integrated sea ice growth anomalies of RASM compared to the mean 2010-2019, are displayed in Figure 7.**

LN 285-286: The sentence was changed to: **The EM ice thickness measurements on board of the Russian icebreaker „Kapitan Dranitzyn“ as part of the MOSAiC resupply between**…

LN 288-290: The sentence was changed to: **The main bias of the EM measurements is connected to the difficulty of instrument calibration on the ramming icebreaker. The frequent ramming operations of the ship with little progress over**

the undisturbed heavy ice makes processing and filtering of the ship-based measurements challenging.

LN297-301: We replotted the satelite picture in Fig. 9 to show the leads north of Spitsbergen more clearly and added red arrows with the word ‚Lead'.

LN 313-329: We revised the 1st part of this paragraph as follows:

Figure 10 displays the anomalies of ice convergence (top), of divergence (middle) and in the bottom panel the ice shear anomaly (all in percent/day) simulated by RASM for the JFM 2020 mean compared to the JFM 2010-2019 mean. In all three plots the transpolar drift in km/day is indicated by thick black arrows. Longer black arrows in the Davis Strait, the east coast of Greenland and the BS indicate individual grid cells with a very different drift. Blue colours in the top part of Fig. 10 indicate regions with reduced convergence and red colours in the middle part of Fig. 10 indicate those with enhanced divergence. These grid cells are likely reflecting the free-drift of thinner sea ice in marginal ice zones, where the impact of atmospheric wind forcing on the ice drift is much less limited compared to the drift within pack ice.

LN 333: OSI-SAF is explained in the text as follows: **The Ocean Sea Ice Satellite Application Facilities (OSA-SAF) deliver satellite derived scatterometer winds, sea surface temperatures and sea ice surface temperatures, radiative fluxes, sea ice concentration, edges, types and sea ice drift.**

Fig. 11 was revised. **The black arrows over the redish shading in the Eastern Arctic indicate the transpolar drift. Longer black arrows in the Davis Strait, the east coast of Greenland and the BS indicate the free-drift of grid cells within marginal ice zones.**

LN: 350: Changed to Bering Strait.

LN 363 and 369: Abbreviations were removed and physical processes are described.

LN: 401-403: Fig. 15 was replotted and enlarged. The mentioned differences at the ice edge region are now clearly visible.

We added the following sentence: **Although the greatest differences occur at the ice edge regions, remarkable changes in the central Arctic, north-west of Greenland, are visible and sea ice volume in this region is to a large extent determined by dynamical processes.**

LN: 416-419:

We added the following sentence:

Comparison of Fig. S10 with Fig. S6 indicates an inverse temperature anomaly pattern between the western and the eastern Arctic for positive and negative AO winters. Under positive AO conditions in winter (Fig. S6 exemplarily for January 2020)) negative temperature anomalies occur over the eastern Arctic and positive anomalies occur over the Canadian Basin in the western Arctic. During the negative AO winter conditions in January 2010 (Fig. S10) the eastern Arctic

reveals weak positive temperature anomalies and the western Arctic negative temperature anomalies.